RSC Advances

PAPER

View Article Online
View Journal | View Issue

Cite this: *RSC Adv.*, 2017, **7**, 15302

$CaCO_3$ thin-film formation mediated by a synthetic protein-lysozyme coacervate†

Chaeyeon Son,‡[a] Sun Young Kim,‡[a] So Yeong Bahn,[b] Hyung Joon Cha[bc] and Yoo Seong Choi*[a]

Received 29th December 2016
Accepted 27th February 2017

DOI: 10.1039/c6ra28808a

rsc.li/rsc-advances

Coacervation is a liquid–liquid phase separation process of macromolecular polyelectrolytes. The formation of simple and complex coacervates of a synthetic acidic protein, GG1234, as a model shell matrix protein, was investigated using turbidity measurements and microscopic morphological observations. Simple coacervation of GG1234 was optimally induced at pH 3.75 and below 50 mM for all of the tested salts, and complex coacervates were prepared at pH 4–9 in sodium acetate solution at various ratios of GG1234 to lysozyme without inducing simple coacervation. The complex coacervates also had the ability to microencapsulate hydrophobic oil droplets in a similar manner to that of other complex coacervation systems. Remarkably, a thin film was formed through *in vitro* $CaCO_3$ crystallization in the presence of complex coacervates, which was expected to be planar and poorly crystalline $CaCO_3$ guided at the interface of two immiscible liquid phases upon complex coacervation. Collectively, our results indicate that our synthetic acidic matrix protein can be used as the main protein for simple and complex coacervations, and the coacervates of this protein may be involved in thin film formation in $CaCO_3$ crystallization.

1. Introduction

Coacervation is a process during which a homogeneous colloidal solution separates into two immiscible liquid phases, a dense liquid phase (coacervate) and a more dilute solution phase and is usually specified as either simple or complex depending on the process that leads to coacervation.[1] Simple coacervation is normally induced by the addition of salts *via* the self-charge neutralization of one type of macromolecule, whereas complex coacervation occurs through associative electrostatic interactions between at least two types of oppositely charged macromolecules.[1,2] Several basic and acidic proteins can serve as biological macromolecules in the formation of coacervates *via* protein–polysaccharide interactions and/or protein–protein interactions, which form various supramolecular structures in biological systems.[3,4] Coacervation has been identified as a possible route for the compartmentalization of biological molecules.[5] However, studies on protein-based simple coacervation and protein–protein complex coacervation are relatively scarce, and a more fundamental understanding of the process and applied studies are needed.

Biomineralization, as the biogenic formation of inorganic materials, is one of the representative biological processes for structural support and protection. Calcium carbonate ($CaCO_3$) biominerals have been relatively well-studied, as one of the most abundant biominerals with superior mechanical and biological properties. An aggregation-based growth mechanism of $CaCO_3$ biominerals has been suggested based on experimental evidence, such as the presence of amorphous precursor phases and nanogranular textures made of oriented nanocrystals less than 100 nm in size.[6] Biopolymers, such as hydrophilic acidic proteins, silk-like proteins and β-chitin, affect the properties of common nanogranular organic/inorganic composite structures in $CaCO_3$ biominerals.[7,8] It has been shown that acidic proteins play important roles in the formation of $CaCO_3$ biominerals, in which less than 5% of the proteins control the shell formation processes of $CaCO_3$ crystal nucleation, growth and regulation in complex shell textures.[9,10] The acidic proteins are mainly composed of amino acids with similar characteristics, such as anionic functional side chains, repetitive sequences, intrinsically disordered protein (IDP) domains and aggregation-prone sequences, even though there are no compositional or structural homologs.[11,12] These sequences can potentially form coacervates and polymer-induced liquid precursors (PILPs) due to the perceived role of polyelectrolytes.[6] We recently produced a recombinant acidic protein (named GG1234) in *Escherichia coli*.[13] The synthetic

[a]*Department of Chemical Engineering and Applied Chemistry, Chungnam National University, Daejeon 34134, Republic of Korea. E-mail: biochoi@cnu.ac.kr*

[b]*School of Interdisciplinary Bioscience and Bioengineering, Pohang University of Science and Technology, Pohang 37673, Republic of Korea*

[c]*Department of Chemical Engineering, Pohang University of Science and Technology, Pohang 37673, Republic of Korea*

† Electronic supplementary information (ESI) available. See DOI: 10.1039/c6ra28808a

‡ Equal contribution.

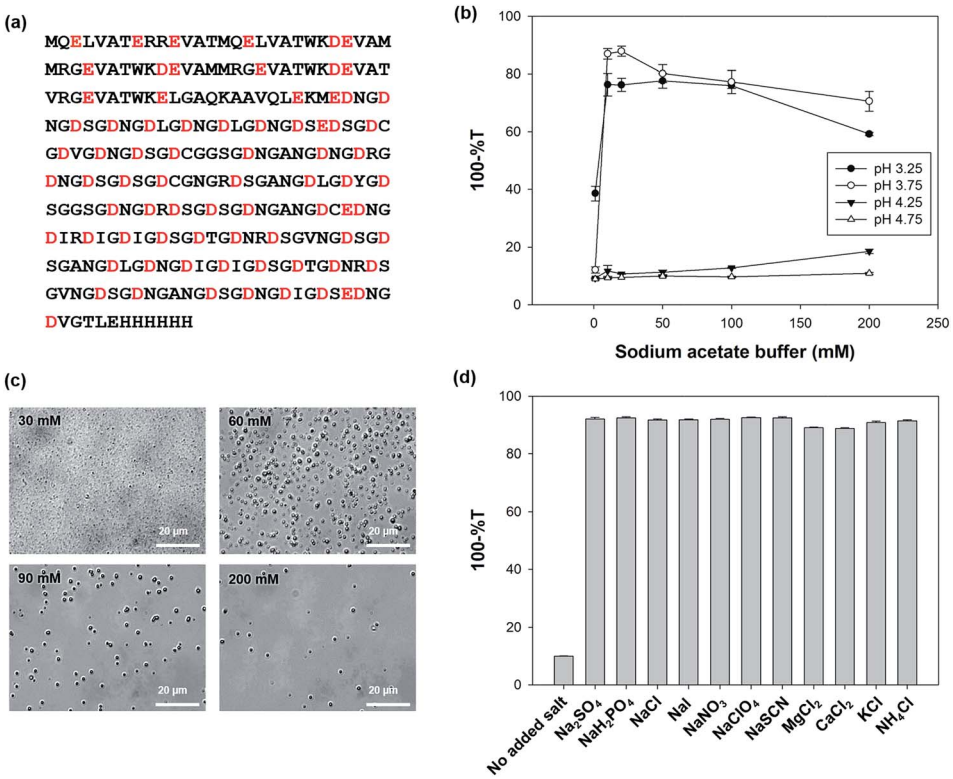

Fig. 1 The effects of pH and salt concentrations on the simple coacervate formation of GG1234 in sodium acetate solution. (a) A schematic representation of the amino acid sequence of GG1234 in which the red letters indicate the acidic amino acid residues. (b) Turbidity measurements of an aqueous GG1234 solution at various pH values and salt concentrations. (c) The optical microscopy images of the morphology of simple coacervates in solutions with various salt concentrations at pH 3.75. (d) Turbidity measurements of the simple coacervate formation of GG1234 in 0.5 mM sodium acetate solution upon the addition of 20 mM of various salts.

protein, GG1234, is composed of acidic and IDP-promoting sequences (Fig. 1a). It has a theoretical pI value of 3.58, efficiently forms a complex with calcium ions and induces spherulitic calcite crystals through the aggregation of nanograins. Similar calcite crystals have been also reported in the presence of double-hydrophilic block copolymers, various polysaccharides and natural shell matrix proteins.[14–17]

In the present study, we found that GG1234 formed simple coacervates with various cationic ions and complex coacervates with lysozyme as a representative basic protein. The hydrophobic model compound was successfully encapsulated with this coacervation system and performed similarly to other coacervation materials, which are often utilized as encapsulation materials for flavors, essential oils and additives in the food industry as well as biocompatible underwater adhesives and potential drug and gene delivery vehicles.[18–20] Finally, this system was applied to *in vitro* $CaCO_3$ crystallization and remarkably guided planar $CaCO_3$ growth at the interface of two immiscible liquid phases of the complex coacervation.

2. Experimental

2.1. GG1234 protein expression and purification

The vector construct for the expression of GG1234 in *E. coli* was previously determined and the protein was expressed and purified based on a previously described method.[13] *E. coli* BL21 (DE3) cells containing the expression vector were grown in Luria–Bertani (LB) medium with 50 μg ampicillin per mL (Sigma-Aldrich, St. Louis, MO, USA) at 37 °C and 200 rpm until the OD_{600} was approximately 0.8. Isopropyl-β-D-thiogalactopyranoside (IPTG; 0.05 mM final concentration; Sigma-Aldrich) was added to induce protein overexpression, and the cells were incubated at 20 °C and 200 rpm for 20 h. The cells were harvested by centrifugation at 8911*g* for 10 min at 4 °C, and the pellets were resuspended in 50 mL lysis buffer (50 mM NaH_2PO_4, 300 mM NaCl and 10 mM imidazole; pH 8.0). The cells were lysed using an ultrasonic cell disrupter (Sonosmasher ULH-700S; Ulsso High-Tech Co., Cheongwon, Korea) at 30% power with a 3 s pulse and a 10 s cooling period between each burst. The lysate was centrifuged at 8911*g* for 10 min at 4 °C. The soluble fraction was collected and applied to Ni–nitrilotriacetic acid (Ni–NTA) resin (Qiagen, Germantown, MD, USA) for affinity purification. After incubating the lysate–Ni–NTA mixture at 4 °C for 1 h, the mixture was loaded onto a column. The resin was washed three times with five column volumes of wash buffer (50 mM NaH_2PO_4, 300 mM NaCl and 20 mM imidazole; pH 8.0). The GG1234 protein was eluted using elution buffer (50 mM NaH_2PO_4, 300 mM NaCl, 300 mM imidazole; pH 8.0) and dialyzed three times in distilled water using a dialysis membrane with a 12–14 kDa molecular weight cut-off

(Spectrum Laboratories Inc., Los Angeles, CA, USA). Finally, the purity was monitored using 12% sodium dodecyl sulfate–polyacrylamide gel electrophoresis (SDS–PAGE), and the protein concentration was assessed using the bicinchoninic acid (BCA) assay method (Sigma-Aldrich).

2.2. Formation of simple coacervates using GG1234

For simple coacervation, GG1234 (1 mg mL^{-1}) was dissolved in sodium acetate solutions of various concentrations (1–200 mM) at different pH values (pH 3.25–4.75). The turbidity of each sample was immediately determined using the absorbance values at 600 nm (SpectraMax 190 microplate reader, Molecular Devices, Sunnyvale, CA, USA) and calculated as 100 − % T (where % T = % transmission = 100×10^{-A}, A = absorbance) because GG1234 does not absorb light at this wavelength. The morphology of each sample was observed using phase contrast optical microscopy (Eclipse Ni-U, Nikon Instruments Inc., Melville, NY, USA). Various salts (final concentration; 20 mM), including Na_2SO_4, NaH_2PO_4, NaCl, NaI, $NaNO_3$, $NaClO_4$, NaSCN, $MgCl_2$, $CaCl_2$, KCl, and NH_4Cl, were independently dissolved in 0.5 mM sodium acetate solution at pH 3.75 to investigate the effects of different salts on the formation of simple coacervates. The turbidity was also determined by measuring the optical density at 600 nm.

2.3. Preparation of complex coacervates using GG1234 and lysozyme, and the microencapsulation of *n*-hexadecane based on complex coacervation

For complex coacervation, the oppositely charged polyelectrolytes GG1234 (2 mg mL^{-1}) and lysozyme (2 mg mL^{-1}) were dissolved in 50 mM sodium acetate solution at different pH values (pH 4–9). Various ratios of GG1234 and lysozyme were directly mixed to form complex coacervates at fixed pH values. The turbidity and morphology were determined using the same UV spectrophotometer and optical microscope.

The model core material for microencapsulation was *n*-hexadecane. First, *n*-hexadecane was labeled with a fluorescent dye, Nile red (Sigma-Aldrich), by dissolving the dye in *n*-hexadecane. An aqueous solution of GG1234 (1 mg mL^{-1}) was prepared in a 25 mM sodium acetate solution (pH 5.0). Then, 50 μL of *n*-hexadecane labeled with Nile red was added to 1 mL of the aqueous solution, and the mixture was emulsified by magnetic stirring for 30 min. Then, an aqueous lysozyme solution (4 mg mL^{-1}) was prepared in 25 mM sodium acetate solution (pH 5.0). The lysozyme solution was applied to the emulsified solution. Microencapsulation with an interfacial coacervation was analyzed using optical/fluorescence microscopy (Eclipse Ni-U, Nikon Instruments Inc., Melville, NY, USA). The encapsulated *n*-hexadecane was monitored using the fluorescence emissions of the Nile red label.

2.4. Coacervate-directed *in vitro* $CaCO_3$ crystallization

The effects of the GG1234/lysozyme coacervates on *in vitro* $CaCO_3$ crystallization were investigated using the slow diffusion of $(NH_4)_2CO_3$ vapor in a $CaCl_2$ solution.[17] Complex coacervates of GG1234 and lysozyme with a ratio of 1 : 4 (w/w) were prepared in 25 mM sodium acetate solution (pH 5.0) with 10 mM $CaCl_2$. A glass cover slip (Marienfeld-Superior, Lauda-Königshofen, Germany) was immersed in the coacervate solution to collect $CaCO_3$ crystals or the condensed coacervate phase. The solution was placed in a closed desiccator at 4 °C and solid $(NH_4)_2CO_3$ (2.5 g) was placed at the bottom of the desiccator. After 20 h, the glass cover slip was rinsed with distilled water and dried at room temperature. *In vitro* $CaCO_3$ crystallization was conducted using a 10 mM $CaCl_2$ solution in a 25 mM sodium acetate solution and $(NH_4)_2CO_3$ vapor, and the condensed dense phase of GG1234/lysozyme coacervation was also collected on the glass cover slip under the same conditions without 10 mM $CaCl_2$ as a negative control. For the morphological observations, the samples were observed using optical microscopy (Eclipse Ni-U, Nikon) and then, the samples were gold-coated and imaged using scanning electron microscopy (SEM) with energy dispersive X-ray analysis (EDX) (SNE-4500M; SEC Co., Suwon, Korea). A cross-section of the mineral was obtained and analyzed with focused ion beam scanning electron microscopy (FIB-SEM) with EDX (LYRA3 XMU, TESCAN, Czech Republic). The X-ray diffraction (XRD) patterns of the obtained precipitates were analyzed and recorded on an X-ray diffractometer (D/MAX-2200; Rigaku Co., Tokyo, Japan) using Cu-Kα radiation (λ = 1.5406 Å, 60 kV, 80 mA).

3. Results and discussion

3.1. Formation of simple coacervates using GG1234

Because simple coacervation is mainly induced through self-charge neutralization under different preparation conditions, such as variations in pH, ionic strength, types of ions present, and the addition of organic solvents,[2] we first investigated the effects of varying pH and salt concentrations using the same salt solution. Fig. 1b shows the pH dependence of turbidity for different concentrations of a sodium acetate solution. The formation of GG1234 simple coacervates occurred in pH range of 3–4 and sodium acetate concentrations below 50 mM. Phase-contrast optical microscopy clearly showed spherical droplets in all the samples and we obtained optimal simple coacervates with diameters of approximately 1 μm using a 30 mM sodium acetate solution (pH 3.75) based on the turbidity measurements (Fig. 1b and c). GG1234 had a theoretical pI value of 3.58 and was composed of two intrinsically disordered domains of repetitive and acidic amino acids (N-terminal domain (pI = 4.74); C-terminal domain (pI = 3.16)).[13] Thus, charge neutralization can occur through electrostatic interactions between the two charged domains of GG1234 over this pH range. GG1234 in 0.5 mM sodium acetate solution did not show a significant difference in turbidity, when compared with that observed in distilled water. The Hofmeister series ranks the relative influence of ions in order of their ability to strengthen or weaken the hydrophobic interactions.[21,22] The typical order of the anionic and cationic series are $SO_4^{2-} > H_2PO_4^- > Cl^- > NO_3^- > I^- > ClO_4^- > SCN^-$ and $Mg^{2+} > Ca^{2+} > K^+ > NH_4^+$, respectively. When the effects of salt ions were also investigated through treatment with an additional 20 mM of salts in a 0.5 mM sodium acetate solution (pH 3.75), GG1234 simple coacervation was promoted

for all of the added salts that were tested, including Na_2SO_4, NaH_2PO_4, NaCl, NaI, $NaNO_3$, $NaClO_4$, NaSCN, $MgCl_2$, $CaCl_2$, KCl and NH_4Cl (Fig. 1d). However, it was difficult to see any significant differences or correlations in turbidity among the anionic or cationic salts. We could expect that cationic salts in the solution interact with the anionic amino acids such as aspartate and glutamate in the protein, which increases the hydrophobic interactions of GG1234. The charges on GG1234 cannot be strong enough to precipitate GG1234. Random mixing of GG1234 in the coacervate phase may allow a number of possible rearrangements of molecules and increase the entropy of the solution.[2]

3.2. Preparation of complex coacervates using GG1234 and lysozymes, and the microencapsulation of *n*-hexadecane based on complex coacervation

Lysozyme, as a model protein for complex coacervation, has a strong basic characteristic with a pI of 10.7. It is known that lysozyme induces complex coacervation with milk proteins, β-lactoglobulin, α-lactalbumin, and glycosaminoglycans (GAGs) such as heparin and hyaluronic acid.[3,23,24] Herein, we first investigated the formation of complex coacervates using GG1234 and lysozyme at different pH values because the attractive electrostatic interactions of two oppositely charged macromolecules play a key role in complex coacervation.[3,25] Experiments were performed within the pH range of 4–9 in a 50 mM sodium acetate solution based on the pI values of two proteins without inducing simple coacervation. Complex coacervation was analyzed using turbidimetric titration and phase-contrast optical microscopy. Overall, the optimum mixing ratio of GG1234 to lysozyme appeared to be insensitive to pH and was broadly determined to be 20 to 60 wt% (Fig. 2a). Spherical droplets of complex coacervates were observed in all of the samples. The diameters of these droplets were approximately 1–5 μm (Fig. 2b). The complex coacervation was not separated immediately into two immiscible phases as a result of droplet coalescence, although it would appear that the droplets coalesce. In the acidic pH range, the net negative charges on GG1234 increased with pH due to the pI value (3.58) of GG1234, whereas the net positive charges on lysozyme (pI = 10.7) were relatively conserved. Thus, the mixing ratio for maximum turbidity could be decreased by increasing the pH. However, the effect was not observed in the pH range of 7–9. When the secondary structure was estimated from the circular dichroism spectrum, GG1234 contained a large amount of random coils and β-strand structures (ESI Fig. 1†). The characteristic structure of GG1234 with two distinct domains (pI = 3.16 and pI = 4.74) and IDP-promoting sequences may influence the differences in the acidic pH range.

Interfacial coacervation was found to be as appropriate for micro-encapsulation of hydrophobic biologically active compounds and phase change materials as an oil-in-water colloidal system.[26,27] *n*-Hexadecane was used as the model hydrophobic core material for microencapsulation, and Nile red was dissolved in *n*-hexadecane for efficient monitoring by fluorescence emission spectroscopy. We applied one of the optimal coacervation conditions discussed above (the 1/4 mixing ratio of GG1234/lysozyme at pH 5.0) in the microencapsulation of *n*-hexadecane. Fig. 3 shows the optical and fluorescent images of the microcapsules prepared using GG1234/lysozyme interfacial coacervation. The sizes of the spontaneously formed microcapsules were approximately 1–10 μm in diameter. On the other hand, fluorescent microcapsules were not observed without the interfacial coacervation process and *n*-hexadecane with Nile red. The results showed that the GG1234-based complex coacervates could be used for coating materials with relatively hydrophobic core materials as with other coacervation systems that have very low interfacial tension with water and behave like viscous particles.[25,28]

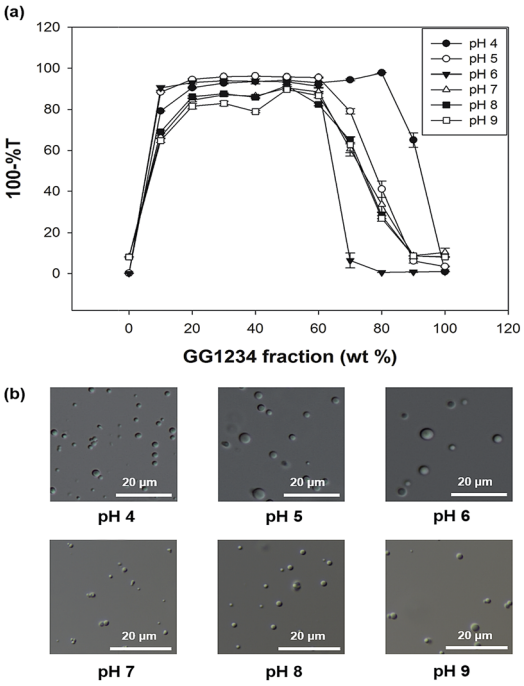

Fig. 2 The preparation of complex coacervates using GG1234 and lysozyme. (a) The effect of pH on the complex coacervation of GG1234 with lysozyme in a 50 mM sodium acetate solution. (b) Optical microscopy images of the morphology of the complex coacervates at various pH values. The ratios of GG1234 and lysozyme were 4 : 1 at pH 4; 2 : 3 at pH 5; 3 : 7 at pH 6 and 1 : 4 at pH 7–9.

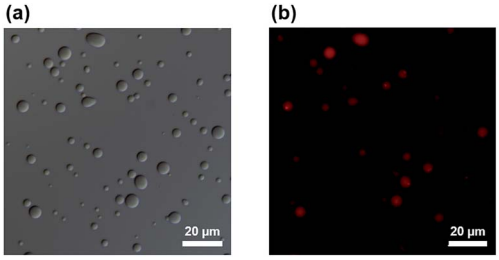

Fig. 3 Optical (a) and fluorescent (b) microscopy images of the *n*-hexadecane droplets microencapsulated by a GG1234/lysozyme complex coacervation. The *n*-hexadecane was labeled with Nile red for fluorescence emission monitoring.

3.3. *In vitro* $CaCO_3$ crystallization based on a GG1234/lysozyme interfacial coacervation

In our previous study, GG1234 induced spherulitic calcite crystals composed of nanograin aggregates.[13] In this study, we applied GG1234-based coacervates to *in vitro* $CaCO_3$ crystallization using a $(NH_4)_2CO_3$ vaporization method. When 10 mM $CaCl_2$ solution was placed in a closed desiccator with a $(NH_4)_2CO_3$ solid powder, characteristic rhombohedral calcite particles were formed with sizes of 20–30 μm in the absence of GG1234 and lysozyme (Fig. 4a), and rosette-like $CaCO_3$ crystals with surfaces of rhombohedral calcitic subunits were observed in the 1 mg mL^{-1} GG1234 solution (Fig. 4b). In contrast, the amount of $CaCO_3$ crystals was highly decreased in the presence of complex coacervates of GG1234 and lysozyme. White precipitates were gradually accumulated at the bottom of the reaction vessel, but the amount was not increased any more after overnight incubation. Although the coacervate phase may be metastable, the coacervates were observed in the mineralization solution after 20 h. A thin film with slightly embedded rhombohedral calcite particles formed on the surface of the immersed cover slip (where a crack occurred when the sample was dried) (Fig. 4c). This film was not formed in the complex coacervate solution without the addition of $(NH_4)_2CO_3$ whether or not $CaCl_2$ was added, but only liquid coacervates partially coated the glass surface (Fig. 4d and e). Because lysozyme itself favors the formation of calcite crystalline structures[29,30] and the coacervates were stable at a high pH (pH 8–9) in the $(NH_4)_2CO_3$ vaporization method for *in vitro* $CaCO_3$ crystallization, GG1234 and its coacervate phase could be involved in film formation during *in vitro* $CaCO_3$ crystallization. The peak intensity of the X-ray diffraction (XRD) pattern of calcite precipitates was decreased substantially, which indicated that the film was mainly composed of a poorly crystalline phase (Fig. 4g and h). A cross-section of the plate film was prepared with a focused ion beam (FIB), and the surface and inner structure were analyzed by scanning electron microscopy (SEM) with energy dispersive X-ray analysis (EDX) (Fig. 4f). On the flat film surface, 17.69% nitrogen and 0.42% calcium were detected. The intensity rapidly decreased upon increasing the milling depth from the surface until the calcium amount was depleted (the thickness was 1.51 μm), and other components such as carbon and oxygen gradually disappeared. Similarly, amorphous $CaCO_3$ (ACC) was prepared in other reports using poly(acrylic acid)-based coacervates, which were used for micromolding of $CaCO_3$ into micropatterned casts that yield smooth surfaces.[31,32] From these results, we suggest that a thin film was formed at the liquid–liquid interface of the GG1234/lysozyme complex coacervation that was mainly composed of poorly crystalline $CaCO_3$ and proteins. The amino acid sequence of GG1234 was obtained from the genome sequence of *Gallus gallus* (jungle fowl), which was available from the National Center for Biotechnology Information (NCBI) database but was removed in a recent

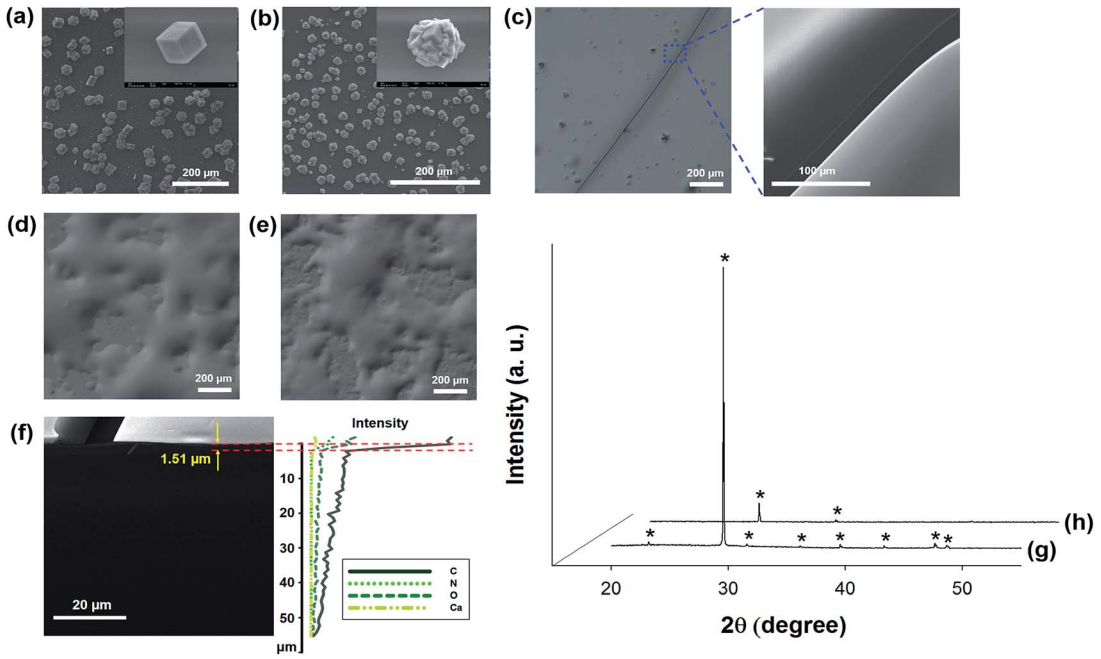

Fig. 4 *In vitro* $CaCO_3$ crystallization based on the GG1234/lysozyme coacervation system. (a) A scanning electron microscopy (SEM) image of *in vitro* $CaCO_3$ crystallization prepared using the $(NH_4)_2CO_3$ vaporization method with no GG1234/lysozyme coacervates. (b) A SEM image of *in vitro* $CaCO_3$ crystallization prepared using the $(NH_4)_2CO_3$ vaporization method in the presence of 1 mg mL^{-1} GG1234. (c) An optical microscopy image of thin film formation during *in vitro* $CaCO_3$ crystallization with the GG1234/lysozyme coacervates. An optical microscopy image of the glass surface coated with GG1234/lysozyme coacervates in the absence (d) and presence (e) of $CaCl_2$. (f) A SEM image and atomic percentage of the surface and cross-section of the plate film prepared using a focused ion beam. The X-ray diffraction (XRD) patterns of $CaCO_3$ precipitates prepared with the $(NH_4)_2CO_3$ vaporization method for samples with no GG1234/lysozyme coacervates (g) and with a thin film formed during *in vitro* $CaCO_3$ crystallization with GG1234/lysozyme coacervates (h).

update of the genome annotation process. Lysozyme is a key component of egg white proteins, and its antimicrobial properties are well characterized.[33] Only sequences of more than 500 eggshell matrix proteins have been identified using a high-throughput tandem-mass spectrometry approach.[33] The synergetic biocomposites of acidic proteins and basic components, such as GG1234 and lysozyme, may have a role in the regulation of eggshell mineralization and antimicrobial defenses, although the interactions and mechanistic details between eggshell matrix proteins and the $CaCO_3$ mineral phase remain unknown.[34,35] In addition, the roles of shell matrix proteins in the biomineralization of various biological systems are not fully understood. The coacervation system based on acidic shell matrix proteins may also be involved in the biomineralization processes combined with polymer-induced liquid precursors (PILPs) as a possible liquid–liquid phase separation event.

4. Conclusions

In this study, simple and complex coacervates were successfully formed based on a synthetic acidic protein, GG1234, which was composed of two distinct domains of repetitive amino acids. A model hydrophobic compound, *n*-hexadecane, was micro-encapsulated by the interfacial coacervation of GG1234 and lysozyme to demonstrate one of the representative properties of coacervation. Remarkably, the coacervates obtained from GG1234 were mainly involved in the formation of a poorly crystalline thin film in *in vitro* $CaCO_3$ crystallization, which was expected due to the properties of GG1234 itself and its coacervate phase. Coacervate formation and the mechanism for its involvement in the formation of thin film surface in *in vitro* $CaCO_3$ crystallization could be interesting, but a deeper understanding of the roles of acidic matrix proteins is be needed. These results suggest that an acidic shell matrix protein may be involved in the formation of simple and complex coacervates, and these coacervates also need to be investigated further to obtain a better understanding of biomineralization behavior in biological systems.

Acknowledgements

This study is supported by the C1 Gas Refinery Program through the National Research Foundation of Korea (NRF) funded by the Ministry of Science, ICT & Future Planning (2016M3D3A1A01913258) and by the Marine Biotechnology program (Marine BioMaterials Research Center) funded by the Ministry of Oceans and Fisheries, Korea.

References

1 W. Zhao and Y. Wang, *Adv. Colloid Interface Sci.*, 2017, **239**, 199–212.
2 A. Gupta and H. B. Bohidar, *Phys. Rev. E: Stat., Nonlinear, Soft Matter Phys.*, 2005, **72**, 011507.
3 T. Croguennec, G. M. Tavares and S. Bouhallab, *Adv. Colloid Interface Sci.*, 2017, **239**, 115–126.
4 A. C. Obermeyer, C. E. Mills, X.-H. Dong, R. J. Flores and B. D. Olsen, *Soft Matter*, 2016, **12**, 3570–3581.
5 C. D. Keating, *Acc. Chem. Res.*, 2012, **45**, 2114–2124.
6 C. Rodriguez-Navarro, E. Ruiz-Agudo, J. Harris and S. E. Wolf, *J. Struct. Biol.*, 2016, **196**, 260–287.
7 S. E. Wolf, C. F. Bohm, J. Harris, B. Demmert, D. E. Jacob, M. Mondeshki, E. Ruiz-Agudo and C. Rodriguez-Navarro, *J. Struct. Biol.*, 2016, **196**, 244–259.
8 L. Addadi, D. Joester, F. Nudelman and S. Weiner, *Chemistry*, 2006, **12**, 980–987.
9 F. Marin, G. Luquet, B. Marie and D. Medakovic, *Curr. Top. Dev. Biol.*, 2008, **80**, 209–276.
10 M. L. H. Rose and M. T. Hincke, *Cell. Mol. Life Sci.*, 2009, **66**, 2707–2719.
11 M. Wojtas, P. Dobryszycki and A. Ozyhar, in *Advanced Topics in Biomineralization*, ed. J. Seto, InTech, 2012.
12 A. Picker, M. Kellermeier, J. Seto, D. Gebauer and H. Colfen, *Z. Kristallogr.*, 2012, **227**, 744–757.
13 C. Son, W. Song, D. S. Hwang, Y. K. Hong, J. Joo and Y. S. Choi, *Korean J. Chem. Eng.*, 2016, **33**, 2406–2410.
14 M. F. Butler, N. Glaser, A. C. Weaver, M. Kirkland and M. Heppenstall-Butler, *Cryst. Growth Des.*, 2006, **6**, 781–794.
15 W. Li and P. Y. Wu, *CrystEngComm*, 2009, **11**, 2466–2474.
16 S. H. Yu, H. Colfen, J. Hartmann and M. Antonietti, *Adv. Funct. Mater.*, 2002, **12**, 541–545.
17 W. Song, S. Y. Bahn, H. J. Cha, S. P. Pack and Y. S. Choi, *Biotechnol. Lett.*, 2016, **38**, 809–816.
18 N. R. Johnson and Y. D. Wang, *Expert Opin. Drug Delivery*, 2014, **11**, 1829–1832.
19 R. J. Stewart, C. S. Wang and H. Shao, *Adv. Colloid Interface Sci.*, 2011, **167**, 85–93.
20 Z. B. Xiao, W. L. Liu, G. Y. Zhu, R. J. Zhou and Y. W. Niu, *J. Sci. Food Agric.*, 2014, **94**, 1482–1494.
21 F. Hofmeister, *Arch. Exp. Pathol. Pharmakol.*, 1888, **24**, 247–260.
22 Y. Zhang and P. S. Cremer, *Curr. Opin. Chem. Biol.*, 2006, **10**, 658–663.
23 S. G. Anema and C. G. de Kruif, *J. Colloid Interface Sci.*, 2013, **398**, 255–261.
24 M. Weert, M. B. Andersen and S. Frokjaer, *Pharm. Res.*, 2004, 2354–2359.
25 C. G. de Kruif, F. Weinbreck and R. de Vries, *Curr. Opin. Colloid Interface Sci.*, 2004, **9**, 340–349.
26 C. Y. Zhao and G. H. Zhang, *Renewable Sustainable Energy Rev.*, 2011, **15**, 3813–3832.
27 C. Schmitt, C. Sanchez, S. Desobry-Banon and J. Hardy, *Crit. Rev. Food Sci.*, 1998, **38**, 689–753.
28 J. Qin, D. Priftis, R. Farina, S. L. Perry, L. Leon, J. Whitmer, K. Hoffmann, M. Tirrell and J. J. de Pablo, *ACS Macro Lett.*, 2014, **3**, 565–568.
29 X. Wang, H. Sun, Y. Xia, C. Chen, H. Xu, H. Shan and J. R. Lu, *J. Colloid Interface Sci.*, 2009, **332**, 96–103.
30 A. E. Voinescu, D. Touraud, A. Lecker, A. Pfitzner, W. Kunz and B. W. Ninham, *Langmuir*, 2007, **23**, 12269–12274.
31 V. Lauth, M. Maas and K. Rezwan, *J. Mater. Chem. B*, 2014, **2**, 7725–7731.

32 P. Kaempfe, V. R. Lauth, T. Halfer, L. Treccani, M. Maas and K. Rezwan, *J. Am. Ceram. Soc.*, 2013, **96**, 736–742.
33 K. Mann, B. Macek and J. V. Olsen, *Proteomics*, 2006, **6**, 3801–3810.
34 M. T. Hincke, Y. Nys, J. Gautron, K. Mann, A. B. Rodriguez-Navarro and M. D. McKee, *Front. Biosci., Landmark Ed.*, 2012, **17**, 1266–1280.
35 Y. Nys, J. Gautron, J. M. Garcia-Ruiz and M. T. Hincke, *C. R. Palevol*, 2004, **3**, 549–562.